Kinetic Monte Carlo and cellular particle dynamics simulations of multicellular systems

Elijah Flenner, Lorant Janosi, Bogdan Barz, Adrian Neagu, Gabor Forgacs, and Ioan Kosztin

Phys. Rev. E **85**, 031907 — Published 8 March 2012

DOI: 10.1103/PhysRevE.85.031907

Kinetic Monte Carlo and Cellular Particle Dynamics Simulations of Multicellular Systems

Elijah Flenner,[1] Lorant Janosi,[1] Bogdan Barz,[1] Adrian Neagu,[1,2] Gabor Forgacs,[1,3,4] and Ioan Kosztin[1,*]

[1] *Department of Physics and Astronomy, University of Missouri, Columbia, MO 65211*
[2] *Department of Biophysics and Medical Informatics, University of Medicine and Pharmacy Timisoara, 300041 Timisoara, Romania*
[3] *Department of Biological Sciences, University of Missouri, Columbia, MO 65211*
[4] *Department of Biomedical Engineering, University of Missouri, Columbia, MO 65211*

Computer modeling of multicellular systems has been a valuable tool for interpreting and guiding *in vitro* experiments relevant to embryonic morphogenesis, tumor growth, angiogenesis and, lately, structure formation following the printing of cell aggregates as bioink particles. Here we formulate two computer simulation methods: (1) a kinetic Monte Carlo (KMC), and (2) a cellular particle dynamics (CPD) method that are capable of describing and predicting the shape evolution in time of 3D multicellular systems during their biomechanical relaxation. Our work is motivated by the need of developing quantitative methods for optimizing post printing structure formation in bioprinting-assisted tissue engineering. The KMC and CPD model parameters are determined and calibrated by using an original computational-theoretical-experimental framework applied to the fusion of two spherical cell aggregates. The two methods are used to predict the: (1) formation of a toroidal structure through fusion of spherical aggregates, and (2) cell-sorting within an aggregate formed by two types of cells with different adhesivities.

PACS numbers: 87.17.Aa, 87.17.Rt, 87.85.G-, 87.85.Lf

I. INTRODUCTION

Understanding how living cells form tissues and organs is a fundamental problem of developmental biology [1, 2], and is also important for the rapidly expanding field of tissue engineering that aims at building functional tissue substitutes *in vitro* [3]. Tissue engineered structures may be used for drug testing and to restore or replace damaged tissues and organs [4]. An emerging tissue engineering technique is bioprinting [5–11] via the automated layer-by-layer deposition of multicellular aggregates (the bioink). Subsequent postprinting fusion of the contiguous aggregates gives rise to the desired tissue construct. Predicting the result of post-printing tissue formation is a task for theoretical modeling.

In general, existing theoretical and computational models of multicellular systems have been restricted to interpret specific shape-forming morphogenetic or other developmental processes. As examples, Odell and coworkers represented the cell as a collection of coupled viscoelastic elements to model gastrulation [12]. Drasdo and Forgacs used the interplay of genetic and generic, physical mechanisms to model blastula formation and gastrulation [13]. Glazier and Graner built a cell as a collection of contiguous spins, defined on a discrete lattice (Cellular Potts Model), and were able to give an account of cell sorting [14, 15]. Palsson and Othmer considered cells as deformable viscoelastic ellipsoids and studied how the motion of individual cells leads to the collective motion of an aggregate of cells [16]. Brodland and coworkers introduced a cell-level finite element method for modeling the forces and the resulting dynamics in 3D multicellular systems [17–19]. Recently, Newman introduced a subcellular element model [20] to study cell division, adaptive cellular shape deformations and primitive streak formation [21–24].

A guiding principle for most models of cell rearrangement in cell aggregates is the *differential adhesion hypothesis* (DAH) proposed by Steinberg [25, 26]. DAH states that structure formation in multicellular systems occurs due to (i) differences in cell-to-cell adhesion of different types of cells and (ii) cell motility. Cells seek positions with the largest number of strong bonds. For example, in a random mixture of two cell types of different cohesivities the more cohesive cell population sorts out and occupies the central region surrounded by the less cohesive population, in analogy with two immiscible liquids of different surface tension. Based on DAH, Steinberg introduced the concept of tissue surface tension, a quantity that was used to provide a quantitative characterization of cell sorting [27]. Recently, it has been proposed that tissue surface tension results from the interplay of differential adhesion and differential tension [17, 28–32].

The purpose of this paper is to formulate two computer simulation methods: (1) a *kinetic Monte Carlo* (KMC), and (2) a *cellular particle dynamics* (CPD) method that are capable of describing and predicting the shape evolution in time of 3D multicellular systems during their biomechanical relaxation. Our work is motivated by the need of developing quantitative methods for optimizing post-printing structure formation in bioprinting-assisted tissue engineering. In the KMC method the configuration of the multicellular system is propagated in time through a standard rejection-free kinetic Monte Carlo algorithm.

* kosztini@missouri.edu

This approach should provide a more accurate description of the time evolution of a multicellular system than other grid based methods, such as, the Metropolis Monte Carlo (MMC) model [6, 33] or the widely used cellular Potts model (CPM). The latter uses a modified MMC algorithm to update the configuration of the simulated system and postulates that time is proportional to the number of MC steps, which in general is not the case [34]. In the CPD method [34] individual cells are modeled as an ensemble of cellular particles (CPs) that interact via short range contact interactions, characterized by an attractive (adhesive interaction) and a repulsive (excluded volume interaction) component. CPs in a cell are held together by an additional confining potential that mimics the role of the cell membrane. The time evolution of the spatial conformation of the multicellular system is determined directly by recording the trajectories of all CPs by integrating their equations of motion. What sets apart CPD from the other similar off-grid particle methods, such as Newman's *subcellular element method* (SEM) [20, 21, 23, 24], is the employed force field (especially the confining potential) and its parametrization that makes the system behave as a complex viscous liquid.

The KMC and CPD model parameters are determined and calibrated by using an original computational-theoretical-experimental framework applied to the fusion of two spherical cell aggregates. In particular, the CPD model parameters are determined such that the shape of two fusing spherical aggregates in the CPD simulation match as closely as possible the one observed experimentally, i.e., two attached spherical caps (see Fig. 1) [35]. For the theoretical description of the fusion of two identical spherical aggregates we use a simple continuum model introduced by Frenkel [36] and further developed by others working in the field of rheology [37, 38]. It is this theoretical continuum model that provides the link between the time scales of simulations and the time scales of experiments. Once this link is established, the KMC and CPD simulations are used to quantitatively predict the time evolution of complex postprinted structures whose description using a continuum hydrodynamics approach is impractical. After calibration, the KMC and CPD models are applied to predict the: (1) formation of a toroidal structure through fusion of spherical aggregates [39], and (2) cell-sorting within an aggregate formed by two types of cells with different adhesivities, two morphogenetic processes [40] driving postprinting structure formation.

The remainder of the paper is organized as follows. Section II describes the KMC (Sec. II A) and the CPD (Sec. II B) methods, as well as the theoretical aspects of the continuum approach of aggregate fusion (Sec. II C). Section III contains the results and discussion of our KMC and CPD simulations, i.e., fusion of identical spherical multicellular aggregates (Sec. III A) and cell sorting (Sec. III B). Conclusions are presented in Sec. IV.

II. COMPUTER AND THEORETICAL MODELING

A. Kinetic Monte Carlo for Multicellular Systems

The Kinetic Monte Carlo method (KMC) was proposed as an alternative to the MMC method for simulating the evolution of Ising models [41]. When a system approaches equilibrium, or is in a metastable state, the Metropolis algorithm rejects most trial moves because the acceptance probability is small. A main feature of the KMC algorithm is that it is "rejection-free". In each step, one calculates the transition rates for all possible changes compatible with the current configuration, and then chooses a new configuration with a probability proportional to the rate of the corresponding transition.

We designed and implemented a KMC algorithm to simulate the time evolution of a lattice model of multicellular systems. Aggregates of cells in cell culture medium are represented on a 3D hexagonal close-packed lattice by associating each site to either a cell or to a similar sized volume element of medium. Thus, the lattice spacing is equal to one cell diameter. We assume that each cell interacts with its 12 nearest neighbors (1st and 2nd neighbors considered to be nearest neighbors) located at a distance of one lattice spacing from the given cell. Interactions are expressed in terms of works of cohesion and adhesion [42, 43], defined as the work needed to break up the contact between two neighbors of respectively similar or differing types of cells. For example, in case of a multicellular aggregate composed of a single cell type, the work needed to extract a cell from the aggregate (i.e. model tissue) is the work of cohesion, ϵ_{cc}, multiplied by the number of the cell's nearest neighbor. The interaction between cells and the cell culture medium is set to zero. The movement of cells is described by assigning rates to swapping cells with adjacent cells of different type and/or with medium elements. These elementary moves occur with rates given by

$$k = w_0 e^{-E_\mathrm{b}/E_T}, \tag{1}$$

where the factor w_0 is the frequency of attempts to cross the energy barrier of height E_b, and E_T is the energy of biological fluctuations [44], the analog of the energy of thermal fluctuations, $k_B T$ (k_B is Boltzmann's constant and T is the absolute temperature). It has been argued that E_T is a characteristic measure of cell motility: the higher is E_T in comparison to the energies of cohesion/adhesion, the higher is the motility of the cell [44].

Due to the complexity of the cytoskeletal machinery responsible for cell movement, there is no unique way to assign a barrier height to the swapping of two cells. Any reasonable choice, however, needs to be consistent with the following set of experimental observations on cell movement in 3D:

(1) Relocation of cells in embryonic tissues and in some

engineered tissues (such as cell aggregates) occurs according to DAH [26, 45]: cells take advantage of their motility to establish the maximum number of strong bonds with their neighbors.

(2) Anchorage-dependent cells do not spontaneously dissociate from the cell aggregate they are part of [26].

(3) The speed of cell movement in 3D matrices has a particular dependence on the strength of cell-matrix adhesion: cell movement is fastest at an optimal strength of binding. Too weak or too strong binding hampers cell movement [46, 47].

Consider a binary particle model for a multicellular system formed by two cell types, $t = 1, 2$ (for a multicellular aggregate composed of one cell type, $t = 1$, surrounded by tissue culture medium, $t = 2$ represents the medium particle). The configurational energy (or total interaction energy), E is expressed as [6]

$$E = \gamma_{12} N_{12} + const, \tag{2}$$

where $\gamma_{12} = (\epsilon_{11} + \epsilon_{22})/2 - \epsilon_{12}$, with ϵ_{11} and ϵ_{22} being the energies of cohesion respectively for cell type 1 and 2, and ϵ_{12} is the energy of adhesion. $N_{12} = \sum_{i=1}^{N_1^I} n_{i2} = \sum_{i=1}^{N_2^{II}} n_{i1}$ is total number of nearest neighbor pairs of different cell types cells, n_{i2} (n_{i1}) the number of nearest neighbors of cell i of type 1(2), which are of type 2(1) and N_1^I (N_2^{II}) the total number of cells of type 1(2), which have at least one (nearest) neighbor of type 2(1). (As the *const* is irrelevant for the evolution of the system, we set it to zero [6].)

Consider two nearest neighbor cells, i and j of different types (without loss of generality we can set $i = 1$ and $j = 2$). The system evolves in time towards configurations of decreasing energy E, i.e. for $\gamma_{12} > 0$ ($\gamma_{12} < 0$) N_{12} decreases (increases). For $\gamma_{12} > 0$ and $\gamma_{12} < 0$ cells respectively phase separate (cell sorting) and mix (cell mixing). Elementary KMC moves consist of swapping two neighbors of different types (swapping cells of same type does not change the energy). The contribution of two such cells, i and j to E is

$$E_{ij} = \frac{1}{2}(n_{i2} + n_{j1}), \tag{3}$$

and $E = \sum_{i=1}^{N_1^I} \sum_{j=1}^{N_2^{II}} E_{ij}$. Furthermore, the larger is E_{ij} the more likely is the KMC move to swap cells i and j. Thus it is reasonable to define the energy barrier $E_{\rm b}^{ij}$ in Eq. (1), for a transition involving the swapping of two cells i and j, as

$$0 \leq E_{\rm b}^{ij} = E_{ij}^{max} - E_{ij}, \tag{4}$$

where E_{ij}^{max} is the maximum possible value of E_{ij}. For $\gamma_{12} > 0$, E_{ij}^{max} is obtained when the number of neighbors of differing type surrounding cells i and j is maximal.

Now we can formulate the steps of our KMC algorithm for simulating the time evolution of multicellular systems: (S1) Set $t = 0$; (S2) Find all interfacial cells (i.e., cells in contact with cell culture medium or with cells of different type) and compute the rates k_m, $1 \leq m \leq M$, corresponding to all possible M transitions involving these cells; (S3) Calculate the cumulative rates: $K_m = \sum_{n=1}^{m} k_n$, $1 \leq m \leq M$; (S4) Generate a uniform random number u between 0 and 1 and carry out event "m" for which $K_{m-1} < uK_M \leq K_m$; (S5) Generate another uniform random number u' between 0 and 1, and increment the time variable (i.e., $t \to t + \Delta t$) by the non-uniform time step

$$\Delta t = -K_M^{-1} \log(u'); \tag{5}$$

(S6) Update all rates k_n that may have changed due to the previous transition "m"; (S7) Return to step S2 and repeat the process until the time variable reaches the desired target value.

B. Cellular Particle Dynamics Method for Multicellular Systems

The *cellular particle dynamics* (CPD) method is an off-lattice, particle-based computer simulation method that can describe and predict the time evolution of 3D multicellular systems during shape changing biomechanical transformations [34]. Within the CPD formalism cells, regarded as continuous objects with self-adaptive shape, are coarse-grained into a finite number, N_{CP}, of equal volume elements. Each volume element is represented by a point-like cellular particle (CP) situated at its center of mass. CPs interact via short-range contact interactions, characterized by an attractive (adhesive interaction) and a repulsive (excluded volume interaction) component. In addition, CPs within a given cell are subject to a confining potential that assures the integrity of the cell. The time evolution of the spatial conformation of the multicellular system is determined directly by calculating the trajectories of all CPs (and, therefore, cells) through integration of their overdamped Langevin equations of motion. This minimalist model, when properly parametrized, has the features of a complex viscous liquid and it is suitable for describing the time evolution of multicellular aggregates and soft-tissue constructs.

For the $n^{\rm th}$ CP in cell α, the equation of motion is

$$\mu \dot{\boldsymbol{r}}_{\alpha_n}(t) = -\nabla_{\alpha_n} U + \boldsymbol{f}_{\alpha_n}(t), \tag{6}$$

where $\boldsymbol{r}_{\alpha_n}(t)$ is the position vector, U is the potential energy function describing the interaction of the CPs , μ is the friction coefficient, $\boldsymbol{f}_{\alpha_n}(t)$ is a random force, and the dot denotes time derivative. The random force is modeled as a Gaussian white noise with zero mean and variance $\langle f_i(t) f_j(0) \rangle = 2D\mu^2 \delta(t) \delta_{ij}$, where D is the sort-time self diffusion coefficient of the CPs. The CPD parameters D and μ are related to the previously introduced

biological fluctuation energy E_T by the Einstein relation $D\mu = E_T$. The CP potential energy U has an intracellular and an inter-cellular component corresponding to CPs belonging respectively to the same cell and to different cells, i.e.,

$$U = \frac{1}{2}\sum_{\alpha}\sum_{\substack{n=1\\ m\neq n}} U^{intra}(|\boldsymbol{r}_{\alpha_n} - \boldsymbol{r}_{\alpha_m}|) + \frac{1}{2}\sum_{\substack{\alpha\\ \beta\neq\alpha}}\sum_{n,m} U^{inter}(|\boldsymbol{r}_{\alpha_n} - \boldsymbol{r}_{\beta_m}|), \tag{7}$$

where α_n (β_m) labels the cellular particle n (m) in cell α (β). We model the short-range contact inter- and intracellular interactions between CPs through

$$U^{inter}(r) = V_{LJ}\left(r; \epsilon^{inter}, \sigma^{inter}\right), \tag{8a}$$

$$U^{intra}(r) = V_{LJ}\left(r; \epsilon^{intra}, \sigma^{intra}\right) + \frac{k}{2}\left(r-\xi\right)^2\Theta(r-\xi), \tag{8b}$$

where

$$V_{LJ}(r;\epsilon,\sigma) = 4\epsilon\left[\left(\frac{\sigma}{r}\right)^{12} - \left(\frac{\sigma}{r}\right)^{6}\right] \tag{8c}$$

is the standard Lennard-Jones potential, and $\Theta(r)$ is the Heaviside step function. Note that instead of V_{LJ} one could use any other potential that has a repulsive core and a short range attractive part. For example, in SEM [20] a Morse potential is used to describe the interaction between two subcellular elements. However, the important addition in CPD is the second quadratic term in U^{intra} that, for $r > \xi$, represents an *elastic confining potential* used to maintain the integrity of the cell. This term, characterized by the elastic constant k, guarantees that the CPs within a cell remain confined inside the boundary of the cell. The time evolution of the multicellular system within the CPD approach is determined by numerically integrating the equations of motion (6) for all CPs. We have accomplished this by implementing the intra- and inter-cellular interaction forces, Eqs. (7)-(8), and a Langevin dynamics integrator in the freely available massively parallel molecular dynamics package LAMMPS [48].

For a multicellular system of a single cell type there are nine CPD model parameters that need to be determined: N_{CP} (the number of CPs per cell), D, μ, σ^{intra}, ε^{intra}, k, ξ, σ^{inter} and ε^{inter}. The choice of N_{CP} is determined by the degree of detail we want to describe individual cells. Since we are interested in the time evolution of the shape of an aggregate formed by a large number of cells and not in the detailed description of the surface dynamics of individual cells, in the present work we make the reasonable choice of $N_{CP} = 10$. Because σ in (8c) determines the size of the interacting CPs, we can set $\sigma \equiv \sigma^{intra} = \sigma^{inter}$. The length ξ in (8b) represents the size (diameter) of a cell, which comprises N_{CP} tightly packed CPs of size σ. Thus, one can estimate $\xi \approx \sigma N_{CP}^{1/3}$.

Next, we define convenient CPD (or computer) length, time and energy units according to

$$\ell_0 = \sigma, \quad t_0 = \frac{\sigma^2}{D}, \quad E_0 = E_T = \mu D. \tag{9}$$

In these units all CPD parameters all pure numbers, and in particular $\sigma = D = \mu = 1$. We set the confining potential parameters as $\xi = 2.5$ ($\sim 10^{1/3}$) and $k = 5$. A larger (smaller) value for k makes the cell more rigid (soft) when subjected to deformations. The chosen value, for which $k\sigma^2/2 = 2.5E_T$, is suitable when cells in the aggregate are exposed only to adhesion and surface tension forces. By choosing $\epsilon^{intra} = 1$ (i.e., same as the biological fluctuation energy E_T) the dynamics of the CPs inside a cell will have sufficient randomness to produce cell surface fluctuations that play an important role in cell motility [49].

Thus, out of the nine CPD parameters we are left with only one, ϵ^{inter}, that needs to be determined such that the time evolution of the shape of the multicellular system follows as closely as possible the corresponding experimental one. For this purpose we focus on the fusion of two identical spherical aggregates, as described in the next section. Based on extensive CPD simulations we have found that the best agreement with experiment is obtained for $1 \leq \epsilon^{inter} < 2$, when the system behaves as a viscous liquid. By increasing ϵ^{inter} above 2 the fusing cellular aggregates show sign of solidification and their behavior deviate significantly from experiment. The results reported in this paper are for $\epsilon^{inter} = 1$. However, these are similar to the ones obtained for any $\epsilon^{inter} < 2$.

Furthermore, in all our CPD simulations we have used an integration time step $\Delta t = 10^{-4}$, and used a cutoff radius $R_c = 2.5$ for $U^{inter}(r)$.

C. Continuum Description of the Fusion of Two Spherical Cell Aggregates

The fusion of two contiguous cell aggregates is driven by surface tension, γ, and resisted by viscosity, η. It is an experimental fact that during the fusion of identical spherical soft tissue aggregates the shape of the system is that of two touching spherical caps (see Fig. 1) [35]. This observation suggests that soft tissues behave like complex viscous liquids whose description requires an a priori unknown hydrodynamic constitutive model. However, the simplicity of the geometry allows us to describe analytically the dynamics of the considered fusion process by employing conservation laws as proposed by Frenkel [36] and Eshelby [50] for the coalescence (sintering) of highly viscous molten drops.

The fusing aggregates are modeled as two spherical caps of radius $R(\theta)$ with circular contact ("*neck*") region of radius $r(\theta) = R(\theta)\sin\theta$ (see Fig. 1A). Volume conservation requires

$$R(\theta) = 2^{2/3}(1+\cos\theta)^{-2/3}(2-\cos\theta)^{-1/3}R_0\ , \tag{10}$$

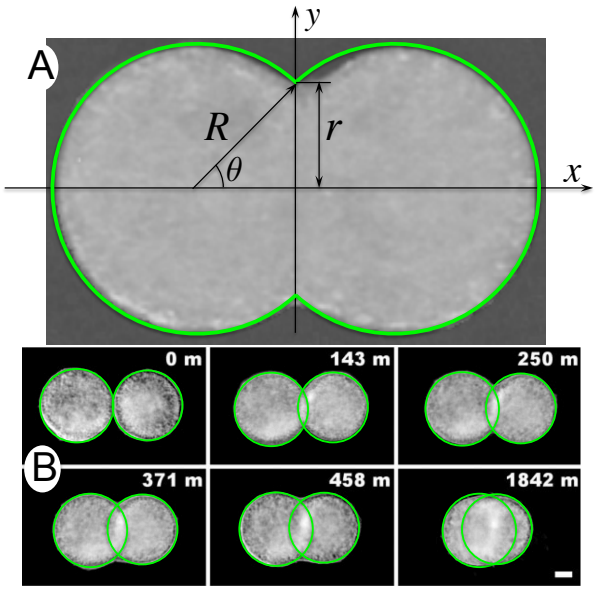

FIG. 1. (color online). (A) The shape of two fusing spherical cell aggregates can be quantified by the angle $\theta(t)$ and the radius $R(t)$. (B) Throughout the fusion of two identical spherical cushion tissue aggregates [35] the system has the shape of two connected spherical caps. The numbers indicate the time (in minutes) elapsed from the start of the fusion.

with $R_0 = R(0)$. Thus, the time evolution of the fusion process is parametrized by a single angle $\theta = \theta(t)$, defined in Fig. 1A, that changes from $\theta(0) = 0$ to $\theta(\infty) = \pi/2$. The rate of the decrease in surface energy is $\dot{W}_s = \gamma dS/dt$, where the free surface area $S = S(\theta) = 4\pi R^2(\theta)(1+\cos\theta)$. The equation of motion for $\theta(t)$ can be derived by equating $\dot{W}_s$ with the rate of the energy dissipated by the viscous flow $\dot{W}_\eta \approx -4\pi R_0^3 \eta \alpha^2$ [36, 38]. Assuming biaxial stretching flow,

$$\alpha = \frac{\partial v_x}{\partial x} \approx -\frac{1}{R(\theta)}\frac{d}{dt}[R(\theta)\cos\theta]. \tag{11}$$

Inserting Eq. (11) into the energy balance equation $\dot{W}_s = \dot{W}_\eta$ leads to [38]

$$\frac{d\theta}{dt} = \frac{1}{\tau}\frac{\sin\theta\cos\theta(2-\cos\theta)^{1/3}}{2^{5/3}(1-\cos\theta)(1+\cos\theta)^{1/3}} = \frac{1}{2\tau}\frac{R_0\cot\theta}{R(\theta)}, \tag{12}$$

where the characteristic fusion time

$$\tau = \eta R_0/\gamma\ . \tag{13}$$

Equation (12) can be solved numerically for $\theta = \theta(t)$. However, one can derive a simple and accurate analytical approximation for $\theta(t)$ by setting $R(\theta) = R_0$ in Eq. (12). Indeed, throughout the fusion process $1 \le R(\theta)/R_0 \le 2^{1/3} \approx 1.26$ holds. With this approximation, Eq. (12) can be easily integrated with the result

$$\cos\theta = \exp(-t/2\tau)\ . \tag{14}$$

Note that according to Eqs. (12) and (14) the dynamics of the fusion process, described by $\theta(t)$ as a function of t/τ, is independent of the size (i.e., R_0) of the fusing spheres. R_0 appears only in the characteristic fusion time τ, Eq. (13).

Finally, using Eq. (14), the square of the radius of the circular neck region of the fusing spherical caps can be expressed as

$$\left(\frac{r}{R_0}\right)^2 \approx A(t)[1-\exp(-t/\tau)]\ , \tag{15a}$$

with

$$A(t) = 2^{4/3}\left(1+e^{-t/2\tau}\right)^{-4/3}\left(2-e^{-t/2\tau}\right)^{-2/3}\ . \tag{15b}$$

For short times, $t \ll \tau$, Eqs. (15) yield the familiar linear-in-time expression, $(r/R_0)^2 \approx t/\tau$, obtained by Frenkel [36] and Eshelby [50].

However, it turns out that instead of Eqs. (15) a more appropriate quantity for describing the shape evolution of the spherical aggregates during the entire fusion process is

$$\left(\frac{r}{R}\right)^2 = \sin^2\theta = 1-\exp(-t/\tau)\ . \tag{16}$$

Indeed, Eq. (16), just like Eq. (14) and unlike Eqs. (15), remains valid even if volume conservation is violated during the fusion process (i.e., when Eq. (10) does not hold). While in CPD and KMC simulations the volume of the system is conserved, in the fusion experiments the volume of the aggregates may change. For example, if the cell cycle time is shorter than the characteristic fusion time τ, one expects the volume of the cell aggregates to increase in the course of fusion due to cell division. As shown in Fig. 1B, during the fusion of cushion tissue aggregates reported in [35], it appears that $R(t) \approx R_0 = \text{const}$, indicating that the volume of the system shrinks, most likely due to cell necrosis. Thus, in this case too, the correct way to determine τ from the experimental data is by employing Eq. (16) instead of Eqs. (15) (see Sec. III A 2).

While the short time limit of Eqs. (15) has been applied previously to estimate the capillary velocity $v_c = \gamma/\eta = R_0/\tau$ of soft tissues [35, 49], we are not aware of any previous study that followed the time evolution of the shape and of $[r(t)/R(t)]^2$ throughout the fusion process of two spherical tissue aggregates. First, we have determined the dimensionless CPD parameters (i.e., expressed in CPD units; see Sec. II B) such that the shape of the fusing aggregates during CPD simulation resemble as close as possible to spherical caps. Second, we have determined the characteristic fusion time τ by fitting the data for $[r(t)/R(t)]^2$, obtained respectively from experiment, CPD and KMC simulations, to Eq. (16). Finally, the CPD time unit can be calculated as $t_0 = \tau_{exp}/\tau_{CPD}$. Once t_0 is known, one can predict through CPD simulation the time evolution of an arbitrary 3D tissue construct built from the same type of cells for which the time

calibration was performed through the above method (i.e., fusion of spherical aggregates). Clearly a similar calibration strategy can be used for the KMC method.

III. RESULTS AND DISCUSSION

To test and compare the KMC and CPD methods described in Sec. II, we have applied them to simulate two important morphogenetic processes: (A) tissue fusion (the fusion of two identical spherical multicellular aggregates), and (B) cell-sorting (within a spherical multicellular aggregate formed by two types of cells with different adhesivities).

A. Fusion of Two Spherical Cell Aggregates

As described in Sec. II C, the fusion of two identical spherical aggregates can quantitatively be characterized by the time dependence of the radius, $r(t)$, of their circular contact region. According to Eq. (16), $r(t)$ obtained from experiment and from KMC and CPD simulations, can be used to determine the characteristic fusion time τ, Eq. (13). Thus, for a given cell type, by comparing the experimental τ with that obtained from computer simulations one can calibrate the time scale of the corresponding computer model. Once such a calibration is done, one can make quantitative *in silico* predictions of the time evolution of various multicellular processes that involve the same cell type [34].

In this section we present KMC and CPD simulation results for the fusion of two identical spherical aggregates. We show that in both cases the computed $(r/R)^2$ vs t/τ dependence can be reasonably well fitted by Eq. (16). Then, using experimental results for aggregate fusion [35], the calibration of the KMC and CPD simulation time scales is exemplified for the case of cardiac cushion tissue (CT). Finally, KMC and CPD simulations are used to predict the formation of a toroidal structure by cell aggregate fusion, an important structure in the engineering of tubular tissue constructs [8].

1. *KMC simulations*

The initial radius of the two identical fusing aggregates used in our KMC simulation was $R_0 = 10$ cell diameters. Each aggregate contained 5,927 cells, with a cell-cell work of cohesion $\epsilon_{cc} = 0.9$. The medium-medium (cell-medium) work of cohesion (adhesion), ϵ_{mm} (ϵ_{cm}), was considered to be negligibly small. A total of 10 KMC simulations of the same fusion process were carried out, each time using a different seed of the random number generator. Each simulation was run for 10^5 KMC time steps.

Representative snapshots during the KMC fusion simulation are shown in Fig. 2. The sought $(r/R)^2$ vs t/τ dependence, obtained by averaging over the 10 KMC simulations, is shown in Fig. 3 (dashed curve). The corresponding standard deviation $\Delta[(r/R)^2]$ was less than 0.04 at all times.

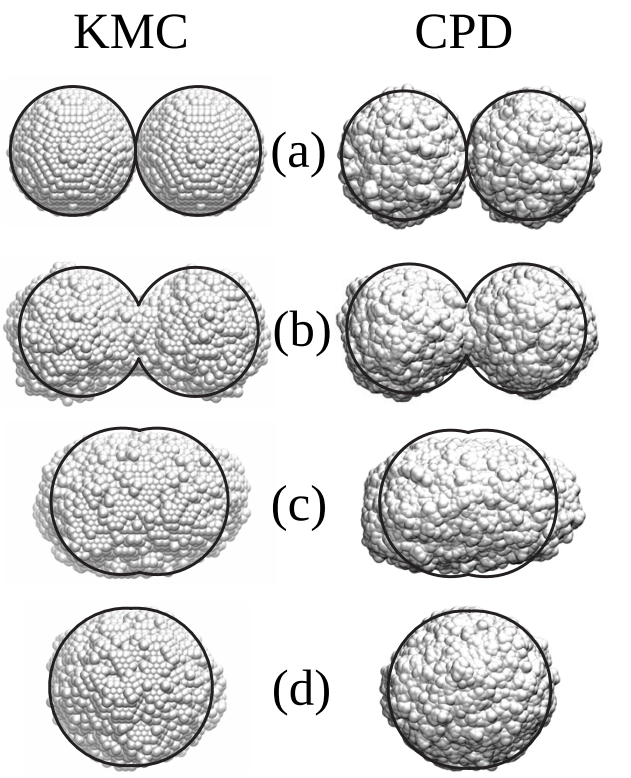

FIG. 2. Time evolution of the fusing aggregates in the KMC (left) and CPD (right) simulations. The snapshots were taken at: (a) $t = 0$, (b) $t = 0.19\tau$, (c) $t = 2.8\tau$, and (d) $t = 5.5\tau$. The solid-line contours represent the theoretical shapes of the fusing aggregates determined by Eqs. (15).

Apart from the beginning of the fusion process (i.e., $t < \tau$) the KMC result appears to match rather well both the theoretical prediction (thick-solid curve), Eq. (16), and the experimental results corresponding to the fusion of CT aggregates (open-circle) [35].

The fusion time in KMC time unit, $t_0 = w_0^{-1}$, obtained by fitting $(r/R)^2$, averaged over the 10 KMC trajectories, to Eq. (16), was $\tau_0 = 1.1 \times 10^9$. Since the experimental characteristic fusion time for CT aggregates $\tau_{exp} \approx 5$h [35], it follows that the KMC time unit (for CT aggregates used in [35]) has the calibrated value $t_0 = w_0^{-1} = \tau_{exp}/\tau_0 = 1.6 \times 10^{-5}$s.

To estimate the relative error $\Delta\tau_0/\tau_0$, first differentiate both sides of Eq. (16) and then replace the differentials with absolute errors, i.e., $\Delta[(r/R)^2] = (t/\tau)\exp(-t/\tau) \cdot (\Delta\tau/\tau) \leq e^{-1}(\Delta\tau/\tau)$, where $e \approx 2.72$. Thus, in general $\Delta\tau/\tau \geq e \cdot \Delta[(r/R)^2]$. For our KMC fusion simulations $\Delta\tau_0/\tau_0 \geq 10\%$.

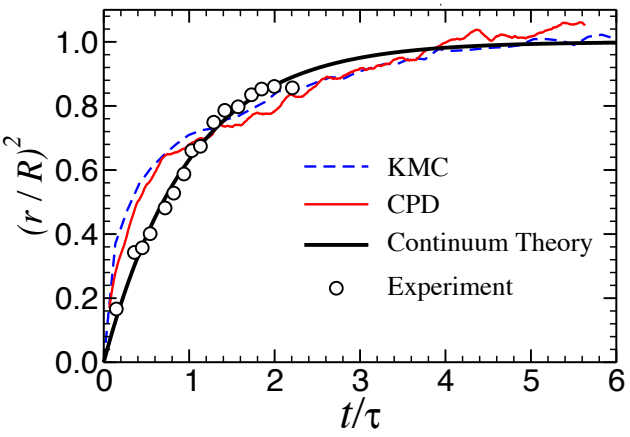

FIG. 3. (color online). Comparison of $(r/R)^2$ vs t/τ for the fusion of two spherical aggregates obtained from KMC simulations (dashed line), CPD simulations (thin solid line), continuum theory (thick solid line) and experiment (circles) using cardiac cushion tissue (CT) aggregates [35].

2. CPD simulations

Each of the two spherical aggregates used in the CPD simulation of aggregate fusion contained 2000 cells. The used CPD parameters and integration timestep, in CPD units, are described in Sec. II B. The equilibrated aggregates were placed within a distance of one σ before starting the fusion simulation.

Representative snapshots during the fusion process are shown, and compared with the corresponding KMC simulation results, in Fig. 2. While in both KMC and CPD simulations the profiles of the fusing aggregates for intermediate stages of the fusion process (Fig. 2b-c) agree quite well, these show noticeable differences with respect to the theoretical prediction, Eq. (16), shown as solid-line contours in Fig. 2.

The $(r/R)^2$ vs t/τ dependence in the CPD simulation is also shown in Fig. 3. The CPD and KMC simulation results are similar. Apart from short times ($t < \tau$) they agree quite well with both the theoretical prediction, Eq. (16), and the experimental results for CT [35].

The characteristic CPD fusion time is determined to be $\tau \approx 540 t_0$. By equating this with $\tau_{\rm exp} \approx 5$h, one finds that the CPD time unit calibrated for CT aggregates is $t_0 \approx 0.6$ min.

To estimate the relative error of τ, we note that $\Delta[(r/R)^2] \approx 2(r/R)^2(\Delta r/r + \Delta R/R) \leq 2(\Delta r/r + \Delta R/R)$. Thus, $\Delta\tau/\tau \geq 5.4 \times (\Delta r/r + \Delta R/R)$. Assuming that both r and R can be determined with a relative error of 1%, one obtains $\Delta\tau/\tau \gtrsim 11\%$, which is similar to the KMC result (see Sec. III A 1).

The CPD simulations were preformed on 32 CPUs of a dual core 2.8GHz Intel Xeon EM64T cluster with a performance of around 5 million timesteps/day (which is equivalent to $500 t_0$ and slightly less than 1τ).

3. Toroidal structure formation

Once the KMC and CPD time scales have been calibrated from the fusion of two spherical CT aggregates, one can employ KMC and CPD simulations to describe and predict the time evolution of more complex CT structures, which are not tractable analytically. To exemplify this point, here we consider the formation of a toroidal structure as a result of the fusion of 10 identical CT spherical aggregates initially arranged in a circular configuration as shown in Fig. 4a. The corresponding KMC and CPD simulations were carried out using the same model parameters as in the fusion of two aggregates described above. In both KMC and CPD simulation the fusion process into a toroidal ring appeared to be completed in $\Delta t \approx 2.5\tau \approx 12.5$ h, as shown in Fig. 4b. This prediction can be tested experimentally by investigating the toroidal structure formation through the fusion of ten spherical, cushion tissue aggregates.

While it seems that both KMC and CPD methods are capable of providing a fairly good description of the shape evolution of a multicellular system during its biomechanical relaxation process, the actual cellular dynamics in the two methods is quite different. Indeed, unlike in CPD simulations, in KMC simulations the motion of individual cells is unrealistically fast. This point is manifest in Fig. 4. By the time the toroidal ring structure is formed, in the KMC simulation, cells from adjacent aggregates (colored differently) appear to be completely mixed. This is clearly not the case in the CPD simulations, where, similarly to existing experimental results [8, 35], there is little mixing between the cells of the fused adjacent aggregates.

To further emphasize this point, we have quantified the degree of cellular mixing during the fusion, along the x-axis, of two identical spherical aggregates [labeled as L (left) and R (right)], with initial radius R_0 (see Fig. 1), by calculating the time dependent mixing parameter

$$d_{mix}(t) = \frac{4}{M}\sum_{m=1}^{M}\frac{\Delta N_m^L(t)\cdot\Delta N_m^R(t)}{[\Delta N_m(t)]^2}. \qquad (17)$$

Here $\Delta N_m^L(t)$ [$\Delta_m^R(t)$] is the number of CPs situated initially (at $t = 0$) in the L (R) aggregate and having, at time t, the $x(t)$ coordinate in the interval $\{-2R_0 + (m-1)\Delta x, -2R_0 + m\Delta x\}$, $1 \leq m \leq M$, with M a properly chosen, sufficiently large integer, $\Delta x = 4R_0/M$, and $\Delta N_m(t) = \Delta N_m^L(t) + \Delta N_m^R(t)$. Clearly, d_{mix} can take values between 0 (completely unmixed system) and 1 (uniformly mixed system).

The time evolution of $d_{mix}(t)$ is shown in Fig. 5. In the KMC simulation cellular mixing is almost complete ($d_{mix} = 1$) after the characteristic fusion time τ, i.e., significantly sooner than the completion of the fusion process ($\sim 6\tau$). By contrast, in the CPD simulation even at the end of the fusion $d_{mix} \sim 0.2 \ll 1$. Based on these results one may conclude that: (i) the cellular dynamics that drives aggregate fusion in the KMC simulations

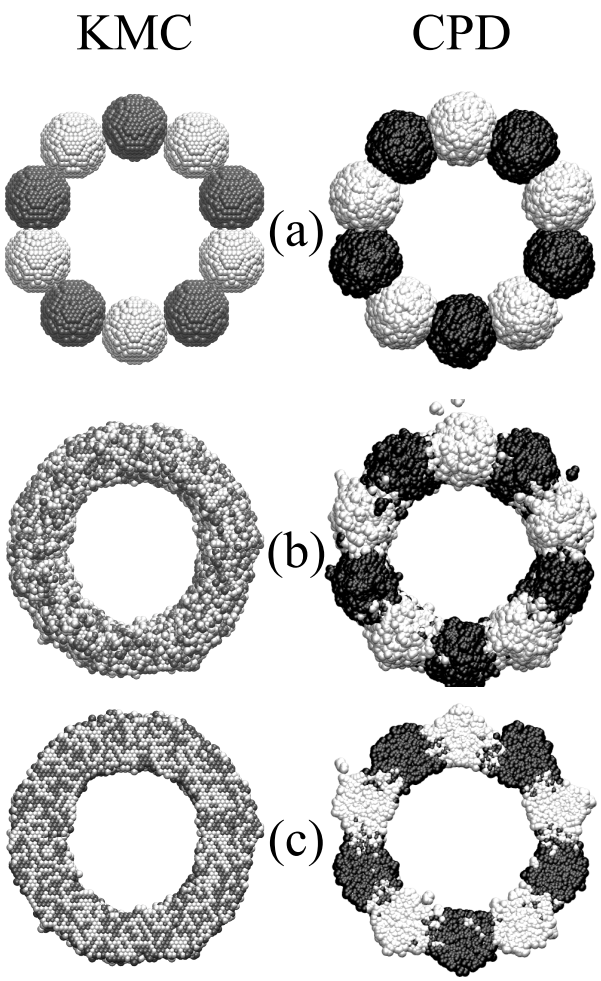

FIG. 4. KMC (left) and CPD (right) simulations of toroidal structure formation through the fusion of 10 cell aggregates. Top view of the fusing aggregates at (a) the beginning ($t = 0$), and (b) the completion of fusion. (c) Cross-section through the median plane of the fused toroidal structure shown in (b). Otherwise identical cells, initially located in adjacent aggregates are colored differently to emphasize the degree of mixing during fusion.

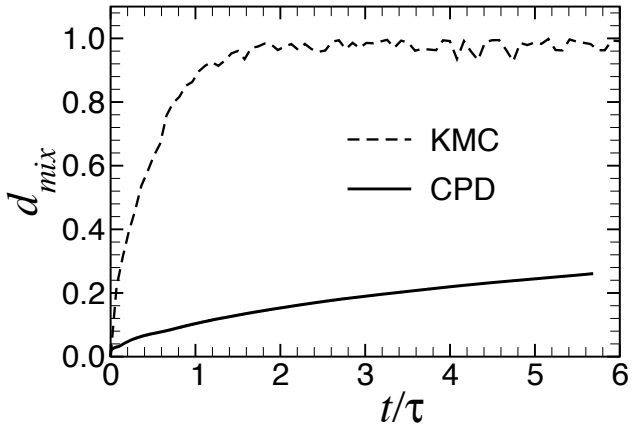

FIG. 5. Time evolution of the mixing parameter d_{mix} calculated for the fusion of two cellular aggregates from the CPD (solid line) and KMC (dashed line) simulations.

is unrealistic (i.e., the system is too liquid-like), and (ii) the CPD model provides a more realistic and attractive approach to describe biomechanical relaxation processes of multicellular systems.

B. Cell Sorting in Two Component Aggregates

When two populations of cells of different adhesivities are randomly mixed within a multicellular aggregate, they sort such that the more adhesive cells occupy the internal region while being surrounded by the less adhesive cells. Cell sorting has been extensively studied both *in vitro* [26, 40, 51, 52] and *in silico* [14, 15, 53].

According to DAH, the outcome of cell sorting in a two-component multicellular aggregate (composed of two types of cells, labeled 'a' and 'b') depends on the relative magnitude of the corresponding works of cohesion/adhesion needed to separate cells of the same/different types (i.e., ϵ_{aa}, ϵ_{bb}, and ϵ_{ab}), respectively [43]. Here we employ both KMC and CPD simulations (described in Secs. II A and II B) to investigate cell sorting in a spherical aggregate of two cell types a and b, with $\epsilon_{aa} < \epsilon_{bb}$. We consider three cases, referred to as C1, C2 and C3, that lead to qualitatively different experimental outcomes [43]. C1: For intermediate adhesion between a and b cells, i.e., $\epsilon_{aa} < \epsilon_{ab} < (\epsilon_{aa}+\epsilon_{bb})/2$, the less cohesive a cells engulf the more cohesive b cells, thus leading to the complete segregation (see Fig. 6b). C2: For strong a–b adhesion, i.e., $(\epsilon_{aa} + \epsilon_{bb})/2 < \epsilon_{ab}$, there is limited sorting and the spherical aggregate remains more or less homogeneously mixed (see Fig. 6c). C3: For weak a–b adhesion, i.e., $\epsilon_{ab} < \epsilon_{aa} < \epsilon_{bb}$, the two types of cells completely separate by transforming the initial spherical aggregate into two attached homogeneous spheroidal caps (each containing either a or b cells) as shown in Fig. 6d. Thus, the degree of cell sorting is enhanced (reduced) for small (large) values of the adhesion energy ϵ_{ab}, compared to the corresponding cohesion energies ϵ_{aa} and ϵ_{bb}. Note that in terms of the interfacial tension γ_{ab} (defined below Eq. (2), for "1" = a and "2" = b), case C1 corresponds to $\gamma_{ab} > 0$ and $\epsilon_{ab} > \epsilon_{aa}$, while case C2 corresponds to $\gamma_{ab} < 0$. The inequalities defining case C3 also imply $\gamma_{ab} > 0$. Thus, in a multicellular aggregate with two types of cells, in order to have cell sorting (segregation) the corresponding interfacial tension must be positive (i.e., $\gamma_{ab} > 0$). The larger this parameter the more efficient and complete the sorting.

The results of our KMC and CPD simulations, presented next, appear to be in good agreement with *in vitro* experimental findings for these three cases [43].

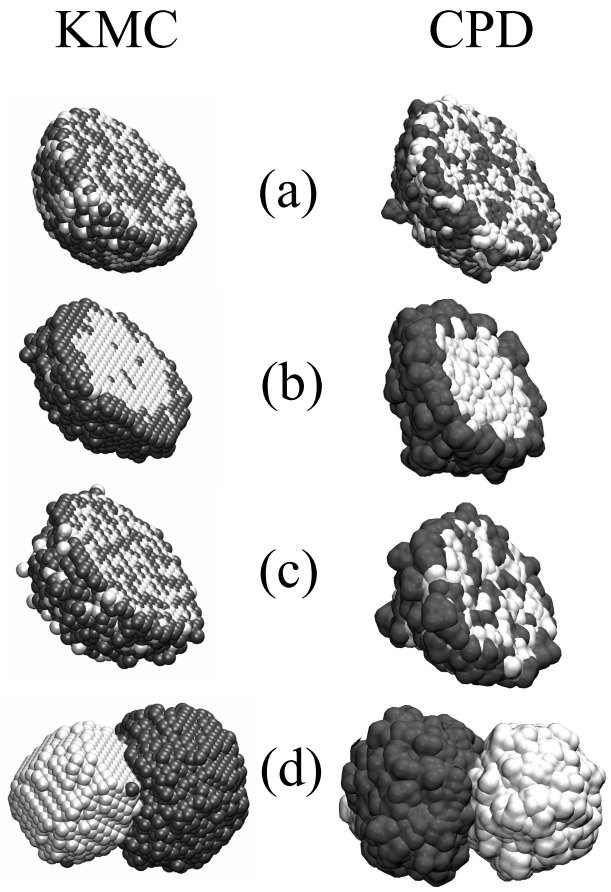

FIG. 6. 3D snapshots from KMC (left) and CPD (right) simulations of the cell sorting in an initially spherical aggregate composed of two randomly mixed cell types (black and light grey). The snapshots represent the (a) initial, and (b-d) final configurations of the simulated system. The latter correspond to (b) intermediate (case C1), (c) strong (case C2), and (d) weak (case C3) cell adhesion energy, as explained in the text. For better visualization of cell mixing/sorting in (a)-(c) only half of the spherical aggregate is shown. (Images rendered with VMD [54]).

1. *KMC simulations*

We have performed three KMC simulations of cell sorting starting with a spherical aggregate composed of a random mixture of $N_a = 3,589$ less cohesive cells of type a and $N_b = 2,362$ more cohesive cells of type b (i.e., with $\epsilon_{aa} < \epsilon_{bb}$). Thus, the spherical aggregate had a total of $N = 5,951$ cells, and a radius of about 10 cell diameters. The values of the model parameters used in the three KMC simulations, corresponding to cases C1, C2 and C3 described above, are listed in Table I. Each KMC simulation was performed up to 10^5 (non-uniform) time steps, given by Eq. (5), leading to the final configurations shown in Fig. 6b-d.

To quantify the degree of cell sorting as a function of time during the KMC simulations, we used a sorting parameter s defined as [55]

TABLE I. Values of the model parameters (energies expressed in units of E_T) used in the KMC and CPD simulations shown in Fig. 6.

Simulation	ϵ_{aa}	ϵ_{ab}	$\frac{\epsilon_{aa}+\epsilon_{bb}}{2}$	γ_{ab}	Case	Outcome
KMC	1.0	1.1	1.4	0.3	C1	Fig. 6b left
KMC	1.0	1.5	1.4	-0.1	C2	Fig. 6c left
KMC	1.0	0.3	1.4	1.1	C3	Fig. 6d left
CPD	0.8	0.9	1.0	0.2	C1	Fig. 6b right
CPD	0.8	1.1	1.0	-0.1	C2	Fig. 6c right
CPD	0.8	0.2	1.0	0.8	C3	Fig. 6d right

$$s = \frac{1}{N}\sum_{i=1}^{N}\frac{N_{t_i}}{N_i}, \tag{18}$$

where N is the total number of cells in the system, and for a given cell i, N_i (N_{t_i}) is the number of nearest neighbor cells regardless of their type (of the same type t_i as the cell i). The sum in Eq. (18) runs over all cells in the system. Clearly, $0 < s < 1$, and the larger s the more complete the sorting. Note that even for completely sorted multicellular systems, built from two (or more) different cell types, the presence of the interface(s) between the segregated regions renders the maximum possible value, s_{max}, of the sorting parameter $s_{max} < 1$. For example, in the above case C1, when at the end of sorting N_a cells of type a completely engulf N_b cells of type b, one can estimate s_{max} as follows. For simplicity, assume that both cell types have spherical shape with the same diameter d. Let ΔN be the number of cells (of either type a or b) situated at the spherical interface, of mean radius R_b and width ΔR, between the two segregated regions (see Fig. 6b), and $N = N_a + N_b$. Since for a cell i situated at the interface $N_{t_i}/N_i \approx 1/2$, according to Eq. (18),

$$s_{max} \approx \frac{1}{N}\left[\frac{1}{2}\times\Delta N + 1\times(N-\Delta N)\right] = 1 - \frac{1}{2}\frac{\Delta N}{N}.$$

Furthermore, assuming that cells are distributed uniformly within the aggregate, one has $N_b(d/2)^3 \approx R_b^3$, i.e., $R_b \approx N_b^{1/3}d/2$, and $\Delta N \times (4\pi/3)(d/2)^3 \approx 4\pi R_b^2 \Delta R$, implying $\Delta N \approx 6N_b^{2/3}(\Delta R/d)$. Finally, assuming that the thickness of the interfacial layer, separating the segregated cell regions, is $\Delta R = xd$, where $2 < x < 3$, one obtains

$$s_{max} \approx 1 - 3x\frac{N_b^{2/3}}{N}. \tag{19}$$

Note that according to Eq. (19), as $N \to \infty$, i.e., for large aggregates, s_{max} approaches unity as $N^{-1/3}$ (assuming that N_a and N_b are of the same order of magnitude).

The time evolution of the sorting parameter, $s = s(t)$, in our KMC simulation corresponding to case C1 is shown

in Fig. 7. The insets represent snapshots of the sorting process taken at times indicated by the arrows.

The sharp increase of $s(t)$ at the beginning of the simulation followed by a slow asymptotic approach to s_{max} indicates that there are at least two sorting time scales. Indeed, the entire time evolution of the sorting parameter can be well fitted with the double exponential

$$s(t) = s_{max} - s_1 e^{-t/\tau_1} - s_2 e^{-t/\tau_2}, \qquad (20)$$

where $s_{max} = 0.76$ is in very good agreement with the theoretically estimated value 0.78 obtained from Eq. (19) for $x = 2.5$. The other fitting parameters in Eq. (20) are: $\tau_1 = 1.4t_0$, $s_1 = 0.27$, $\tau_2 = 58.5t_0$ and $s_2 = 0.11$. The shorter time scale τ_1 corresponds to the local rearrangement (sorting) of cells leading to small clusters of same types of cells, while the longer time scale τ_2 describes the much slower engulfment process of the b cells by the a cells, a process that requires large displacements by a finite number of cells.

Although the results of our KMC simulations appear to be in good qualitative agreement with experiments on cell sorting [25, 26, 43], a quantitative comparison, e.g., in terms of the time evolution of the sorting parameter, is complicated because $s(t)$ is difficult to measure experimentally [56]. Thus, there is no simple way to reliably calibrate the time unit t_0 (which is related to the model parameter w_0) used in the plot of s *vs* t/t_0 in Fig. 7. However, $s(t)$ can also be determined from CPD simulations, thus allowing for a quantitative comparison between the two computer simulation methods.

2. *CPD simulations*

We have also used CPD simulations to investigate cell sorting corresponding to the three cases C1, C2 and C3 described above. The initially spherical aggregate contained a random mixture of equal number $N_a = N_b = 1,000$ of cells of type a and b. While the CPD parameters $\epsilon_{aa} \equiv \epsilon_a^{inter} = \epsilon_a^{intra} = 0.8$ and $\epsilon_{bb} \equiv \epsilon_b^{inter} = \epsilon_b^{intra} = 1.2$ were kept the same in all three simulations, the parameter $\epsilon_{ab} \equiv \epsilon_{ab}^{inter}$ had different values (similar to the ones used in the KMC simulations) for the three cases C1, C2 and C3 as listed in Table I. The cell sorting patterns obtained at the end of the corresponding CPD simulations are shown in Fig. 6. As expected, these patterns are similar to the ones obtained in the KMC simulations.

In order to quantify the degree of cell sorting in the CPD simulations by employing the cell sorting parameter s, defined through Eq. (18), we determined the position of a cell by the center of mass of the constituent CPs, and considered two cells to be neighbors if they were separated by a distance less than 3.25 σ. For the CPD simulation corresponding to case C1, $s(t)$ is shown Fig. 7. Similarly to the KMC result, $s(t)$ can be fitted well with the double exponential (20). Again, $s_{max} = 0.68$ is in good agreement with the theoretical prediction Eq. (19), i.e., 0.67 for $x = 2.2$ (or 0.63 for $x = 2.5$). The other

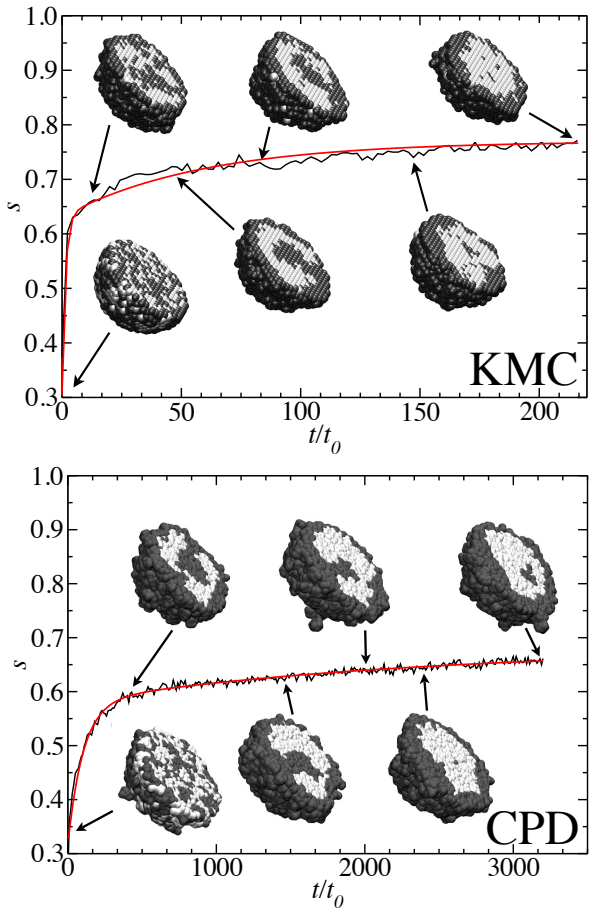

FIG. 7. (color online). Time dependence of the cell sorting parameter, $s = s(t)$, corresponding to case C1 described in the text, for both KMC (top) and CPD (bottom) simulations. The fits (red curves) correspond to Eq. (20), with values of the fitting parameters indicated in the text. The insets represent snapshots of half of the spherical aggregate taken at times indicated by arrows.

fitting parameters in Eq. (20) are: $\tau_1 = 0.68\ t_0$, $\tau_2 = 103\ t_0$, $s_1 = 0.25$ and $s_2 = 0.1$. Note that while s_1 and s_2 have essentially the same values for both KMC and CPD simulations, the time constants τ_1 and τ_2 are quite different, as the corresponding time units t_0 are different in the two simulations. Moreover, the fact that, for similar model parameters, $\tau_2/\tau_1 = 41.8$ in KMC is about twice as large as $\tau_2/\tau_1 = 21.7$ in the corresponding CPD simulation indicates that the self diffusive motion of cells in KMC occurs much faster than in CPD. In other words, the multicellular system is more liquid-like in KMC than in CPD simulations.

IV. CONCLUSIONS

We have formulated two computer simulation methods, KMC and CPD, that are capable of describing

and predicting the shape evolution in time of 3D multicellular systems during their biomechanical relaxation. The KMC and CPD model parameters were determined and calibrated by using an original computational-theoretical-experimental framework applied to the fusion of two spherical cell aggregates. Our study was motivated by the need to quantify biomechanical properties of engineered tissue constructs, composed of compact tissues made of adhesive and motile cells and to predict their time evolution. The growing interest for understanding shape changes in such tissue constructs stems from their applications in tissue engineering in general and in the emergent field of 3D bioprinting in particular [8].

The KMC method is based on a lattice representation of the 3D tissue construct and dynamics is described in terms of rates associated with possible movements of cells. Similarly to previously employed MMC studies, the mixing pattern observed in KMC simulations disagrees with experiments. In both methods an elementary move consists in cells swapping positions with neighbors, which overestimates cell motility. However, with proper time scale calibration, KMC simulations can be used to describe and predict reasonably well the time evolution of the shape of the simulated multicellular system.

The CPD method is based on modeling individual cells in a tissue construct as interacting CPs. The dynamics of the multicellular system are determined by integrating the equations of motion for each CP. The CPD force field parameters are determined such that the time evolution of the shape of the fusing spherical aggregates in the CPD simulation matches as closely as possible the experimental one (i.e., two touching spherical caps). Once the CPD model is calibrated, this can be used to simulate the shape evolution of arbitrary 3D multicellular constructs. It should be emphasized that in CPD (i.e., computer) units the calibrated CPD parameters (and therefore the outcome of a CPD simulation) are independent of the used cell type. However, the CPD units (9) have specific values for different cell types. Thus, the CPD simulations reported here can be applied as is to different cell types; the corresponding CPD time unit t_0 should be determined in each case by equating $\tau_{sim} \approx 540\, t_0$ (see Sec. III A 2) with the experimental fusion time τ_{exp}.

The reported CPD simulations provided a good description for both fusion and cell sorting of multicellular spheroids. We found that CPD provides a more realistic description of complex multicellular structure formation than KMC. Indeed, the behavior of the studied multicellular systems in CPD simulations resembles to that of complex visco-elastic materials while in KMC simulations to that of viscous liquids. It is to be expected that by including more realistic features into the interaction of the CPs the accuracy of the CPD method can be further improved.

ACKNOWLEDGMENTS

This work was supported by grants from the National Science Foundation (PHY-0957914 and FIBR-0526854). The work by A.N. was supported in part by the Romanian National Authority for Scientific Research (CNCSIS Contract PCCE-ID 76). Computational resources were generously provided by the University of Missouri Bioinformatics Consortium.

[1] D. Ingber and M. Levin, Development **134**, 2541 (2007).
[2] G. Forgacs and S. Newman, *Biological physics of the developing embryo* (Cambridge University Press, 2005).
[3] R. Langer and J. P. Vacanti, Science **260**, 920 (1993).
[4] L. G. Griffith and G. Naughton, Science **295**, 1009 (2002).
[5] V. Mironov, T. Boland, T. Trusk, G. Forgacs, and R. R. Markwald, Trends Biotechnol **21**, 157 (2003).
[6] K. Jakab, A. Neagu, V. Mironov, R. R. Markwald, and G. Forgacs, Proc Natl Acad Sci U S A **101**, 2864 (2004).
[7] T. Boland, T. Xu, and X. Cui, Biotechnol J **1**, 910 (2006).
[8] K. Jakab, C. Norotte, B. Damon, F. Marga, A. Neagu, C. L. Besch-Williford, A. Kachurin, K. H. Church, H. Park, V. Mironov, R. R. Markwald, G. Vunjak-Novakovic, and G. Forgacs, Tissue Engineering: Part A **14**, 413 (2008).
[9] V. Mironov, R. P. Visconti, V. Kasyanov, G. Forgacs, C. J. Drake, and R. R. Markwald, Biomaterials **30**, 2164 (2009).
[10] C. Norotte, F. S. Marga, L. E. Niklason, and G. Forgacs, Biomaterials **30**, 5910 (2009).
[11] K. Jakab, C. Norotte, F. Marga, K. Murphy, G. Vunjak-Novakovic, and G. Forgacs, Biofabrication **2**, 1 (2010).
[12] G. M. Odell, G. Oster, P. Alberch, and B. Burnside, Dev Biol **85**, 446 (1981).
[13] D. Drasdo and G. Forgacs, Developmental dynamics : an official publication of the American Association of Anatomists **219**, 182 (2000).
[14] F. Graner and J. A. Glazier, Physical Review Letters **69**, 2013 (1992).
[15] J. A. Glazier and F. Graner, Physical Review E **47**, 2128 (1993).
[16] E. Palsson and H. G. Othmer, Proceedings of the National Academy of Sciences of the United States of America **97**, 10448 (2000).
[17] G. W. Brodland, J Biomech Eng **124**, 188 (2002).
[18] G. W. Brodland, Applied Mechanics Reviews **57**, 47 (2004).
[19] M. S. Hutson, G. W. Brodland, J. Yang, and D. Viens, Physical Review Letters **101**, 148105 (2008).
[20] T. J. Newman, Mathematical Biosciences and Engineering **2**, 611 (2005).
[21] S. A. Sandersius and T. J. Newman, Phys Biol **5**, 15002 (2008).
[22] T. J. Newman, Curr Top Dev Biol **81**, 157 (2008).
[23] S. A. Sandersius, C. J. Weijer, and T. J. Newman, Physical biology **8**, 045007 (2011).

[24] S. A. Sandersius, M. Chuai, C. J. Weijer, and T. J. Newman, Physical biology **8**, 045008 (2011).
[25] M. S. Steinberg, Science **141**, 401 (1963).
[26] M. S. Steinberg, J Exp Zool **173**, 395 (1970).
[27] R. A. Foty, C. M. Pfleger, G. Forgacs, and M. S. Steinberg, Development **122**, 1611 (1996).
[28] M. Krieg, Y. Arboleda-Estudillo, P. H. Puech, J. Kafer, F. Graner, D. J. Muller, and C. P. Heisenberg, Nature cell biology **10**, 429 (2008).
[29] T. Lecuit, HFSP journal **2**, 72 (2008).
[30] T. Lecuit and P. F. Lenne, Nature reviews. Molecular cell biology **8**, 633 (2007).
[31] A. C. Martin and E. F. Wieschaus, Nature cell biology **12**, 5 (2010).
[32] M. L. Manning, R. A. Foty, M. S. Steinberg, and E. M. Schoetz, Proceedings of the National Academy of Sciences of the United States of America **107**, 12517 (2010).
[33] A. Neagu, K. Jakab, R. Jamison, and G. Forgacs, Physical Review Letters **95**, 178104 (2005).
[34] E. Flenner, F. Marga, A. Neagu, I. Kosztin, and G. Forgacs, Curr. Top. Dev. Biol. **81**, 461 (2008).
[35] K. Jakab, B. Damon, F. Marga, O. Doaga, V. Mironov, I. Kosztin, R. Markwald, and G. Forgacs, Developmental dynamics : an official publication of the American Association of Anatomists **237**, 2438 (2008).
[36] J. Frenkel, J. Physics **9**, 385 (1945).
[37] O. Pokluda, C. T. Bellehumeur, and J. Vlachopoulos, Aiche Journal **43**, 3253 (1997).
[38] C. T. Bellehumeur, M. Kontopoulou, and J. Vlachopoulos, Rheologica Acta **37**, 270 (1998).
[39] P. A. Fleming, W. S. Argraves, C. Gentile, A. Neagu, G. Forgacs, and C. J. Drake, Developmental dynamics : an official publication of the American Association of Anatomists **239**, 398 (2010).
[40] J. M. Perez-Pomares and R. A. Foty, Bioessays **28**, 809 (2006).
[41] A. B. Bortz, M. H. Kalos, and J. L. Lebowitz, J Comput Phys **17**, 10 (1975).
[42] J. Israelachvili, *Intermolecular and Surface Forces* (Academic Press, 1997).
[43] R. A. Foty and M. S. Steinberg, Int J Dev Biol **48**, 397 (2004).
[44] D. A. Beysens, G. Forgacs, and J. A. Glazier, Proceedings of the National Academy of Sciences of the United States of America **97**, 9467 (2000).
[45] M. S. Steinberg and T. J. Poole, "Liquid behavior of embryonic tissues," in *Cell Behavior*, edited by R. Bellairs, A. S. G. Curtis, and G. Dunn (Cambridge University Press, 1982) pp. 583–697.
[46] S. P. Palecek, J. C. Loftus, M. H. Ginsberg, D. A. Lauffenburger, and A. F. Horwitz, Nature **385**, 537 (1997).
[47] M. H. Zaman, R. D. Kamm, P. Matsudaira, and D. A. Lauffenburger, Biophysical Journal **89**, 1389 (2005).
[48] S. Plimpton, Journal of Computational Physics **117**, 1 (1995).
[49] R. Gordon, N. S. Goel, M. S. Steinberg, and L. L. Wiseman, J Theor Biol **37**, 43 (1972).
[50] J. D. Eshelby, Trans. AIMME **185**, 806 (1949).
[51] M. S. Steinberg, Proc Natl Acad Sci U S A **48**, 1577 (1962).
[52] M. S. Steinberg, Exp Cell Res **30**, 257 (1963).
[53] J. C. Mombach, J. A. Glazier, R. C. Raphael, and M. Zajac, Physical Review Letters **75**, 2244 (1995).
[54] W. Humphrey, A. Dalke, and K. Schulten, Journal of Molecular Graphics **14**, 33 (1996).
[55] E. Palsson, Future Generation Computer Systems **17**, 835 (2001).
[56] U. Technau and T. W. Holstein, Dev Biol **151**, 117 (1992).